

# Experimental verification of textured mechanical seal designed using multi-objective optimization

*Xiuying Wang*

Nanjing University of Aeronautics and Astronautics, Nanjing, Jiangsu, China

*Michael Khonsari*

Louisiana State University College of Engineering, Baton Rouge, Louisiana, USA

*Siyuan Li and Qingwen Dai*

Nanjing University of Aeronautics and Astronautics, Nanjing, Jiangsu, China, and

*Xiaolei Wang*

College of Mechanical and Electrical Engineering, Nanjing University of Aeronautics & Astronautics, Nanjing, China

## Abstract

**Purpose** – This study aims to simultaneously enhance the load-carrying capacity and control the leakage rate of mechanical seals by optimizing the texture shape.

**Design/methodology/approach** – A multi-objective optimization approach is implemented to determine the optimal “free-form” textures and optimal circular dimples. Experiments are conducted to validate the simulation results.

**Findings** – The experimental coefficient of friction (COF) and leakage rate are in good agreement with the calculated results. In addition, the optimal “free-form” texture shows a lower COF and a lower leakage in most cases.

**Originality/value** – This work provides a method to optimize the surface texture for a better combination performance of mechanical seals.

**Keywords** Multi-objective optimization, Lubrication, Surface texture, Leakage, Mechanical seal

**Paper type** Research paper

## 1. Introduction

There are numerous publications reported that surface texturing is useful for improving the tribological performance of sliding surfaces such as mechanical seals and bearings (Gropper *et al.*, 2016; Gachot *et al.*, 2013; Cem, 2009; Tala-Ighil *et al.*, 2011; Brunetière and Tournier, 2012; Gachot *et al.*, 2017; Shi *et al.*, 2016). Grooves and dimples are common types of surface textures in mechanical seals (Etsion and Burstein, 1996; Kovalchenko *et al.*, 2005; Marian *et al.*, 2007; Galda *et al.*, 2009). An extensive literature reveals that the primary focus of surface texture has been put on the circular dimples (Ahmed *et al.*, 2016; Ibatan *et al.*, 2015; Wan and Xiong, 2008; Qiu and Khonsari, 2011; Wang *et al.*, 2014). Other “regular texture” shapes such as triangle (Yu *et al.*, 2010), ellipse (Qiu and Khonsari, 2011), diamond (Siripuram and Stephens, 2004), square (Rahmani *et al.*, 2007; Uddin *et al.*, 2017; Qiu *et al.*, 2013) and hexagon (Siripuram and Stephens, 2004) have also been studied. For instance, a comparative study of six texture shapes shows that the elliptical shape yields the lowest coefficient of friction and the largest stiffness (Qiu *et al.*, 2013).

With recent advances in optimization techniques, “irregular texture” with more complicated geometric configurations have begun to draw attention. The texture with a chevron shape starting from an arbitrary texture using sequence quadratic program was obtained, and it can provide the largest load-carrying capacity (Shen and Khonsari, 2016). The textures with fish shape and fusiform shape for a lower friction using the genetic algorithm (GA) programming were obtained (Zhang *et al.*, 2017). These studies have provided a path forward for further texture shapes optimization.

Nevertheless, many studies have reported that simultaneously achieving an enhanced load-carrying capacity and decreasing the leakage is not easy to accomplish via surface texturing (Brunetière and Tournier, 2012; Qiu and Khonsari, 2011). The clearance between two rings increases as the load-carrying capacity increases. This will result in an obvious increase of leakage rate. To obtain a better performance of gas face seals, a multi-objective optimization approach combined with the Reynolds equation for the compressible flow was developed to optimize dimple shape (Wang *et al.*, 2018).

The current issue and full text archive of this journal is available on Emerald Insight at: [www.emeraldinsight.com/0036-8792.htm](http://www.emeraldinsight.com/0036-8792.htm)



Industrial Lubrication and Tribology  
71/6 (2019) 766–771  
© Emerald Publishing Limited [ISSN 0036-8792]  
[DOI 10.1108/ILT-11-2018-0398]

This paper is supported by the Funding of Jiangsu Innovation Program for Graduate Education (No. KYLX16\_0326), the Fundamental Research Funds for the Central Universities (No. NZ2016106), the National Nature Science Foundation of China (NSFC) (No. 51675268).

Received 12 November 2018

Revised 17 December 2018

Accepted 17 December 2018

Geometries with an asymmetric ‘V’ shape were reported to have a higher load-carrying capacity and a lower leakage rate.

This paper applies the multi-objective optimization approach to treat a liquid lubricated seal. The optimal sets for ‘free-form’ shape and circular shape were obtained using NSGA-II (elitist non-dominated sorting GA). More detailed information about NSGA-II can be found in previous work (Wang et al., 2018). Specimens with the obtained optimal textures were constructed and tested experimentally to verify the results of the optimization.

## 2. Multi-objective optimization for dimple shape

### 2.1 Multi-objective optimization model

The multi-objective optimization approach for optimizing the ‘free-form’ texture shape and circular shape in the previous paper (Wang et al., 2018) was used to treat a liquid lubricated seal. To simplify the formulation, a single-cell model is used. The goal is to obtain a higher dimensionless load-carrying capacity  $\bar{W}$  and a lower dimensionless leakage rate  $\bar{Q}$ ,  $\bar{W}$  and  $\bar{Q}$  can be expressed, respectively, by:

$$\begin{aligned} W &= \int_0^\varphi \int_{r_1}^{r_o} p r dr d\theta \\ \bar{W} &= \frac{W}{p_a r_1^2} \\ Q &= \int_0^\varphi \left. \frac{\rho r h^3 \partial p}{6 \mu \partial r} \right|_{r=r_1} d\theta \\ \bar{Q} &= \frac{6 \mu}{\rho h_0^3 p_a} Q \end{aligned} \quad (1)$$

The related parameters and their values are listed in Table I.

$\bar{W}$  and  $\bar{Q}$  can be calculated after the film pressure  $p$  is obtained by solving the Reynolds equation. A common and simplified finite differential method was applied to solve the non-dimensional steady-state Reynolds equation, which is similar to the published paper (Shen and Khonsari, 2016). It

Table I Related parameters and their values

Items	Values
Inner radius of rotating ring $r_1$ , mm	17.9
Outer radius of rotating ring $r_2$ , mm	23.4
Inner radius of computational region $r_1$ , mm	19.73
Outer radius of computational region $r_o$ , mm	21.57
Span of computational region $\varphi$ , rad	$\pi/10$
Dynamic viscosity $\mu$ , Pa-s	$40.25 \times 10^{-3}$
Density $\rho$ , g/cm <sup>3</sup>	0.86
Pressure $p_a$ , MPa	0.1
Inner boundary pressure $p_1$ , MPa	0.12
Outer boundary pressure $p_o$ , MPa	0.1
Rotational speed $\omega$ , rad/s	209
Ratio of minimum film thickness to texture depth $h_0/h_g$	1
Texture depth $h_g$ , $\mu\text{m}$	5
Film thickness $h$ , $\mu\text{m}$	$h_g + h_0$ in texture region $h_0$ beyond texture region

can be modified by other factors according to the actual conditions such as thermal effect, flow state, etc.

### 2.2 Optimization results

There is usually not only one solution but also a solution set for a multi-objective optimization problem. Figure 1 shows the optimal ‘free-form’ shapes and optimal circular shapes for the speed of 209 rad/s. The seven solutions can meet different leakage or load-carrying capacity requirements.

Figure 2 shows the multi-objective optimization solutions of the ‘free-form’ shape and the circular shape. Taking the ‘free-form’ shape as an example, the area is divided into two parts by a curve. The optimal solutions for circular shapes are located in the black shadowed area, which means the optimal ‘free-form’ textures can provide a better combination of performances than the optimal circular shapes. For instance, for the optimal Point 4,  $\bar{Q}$  is 68.9, and the corresponding optimal ‘free-form’ texture can provide a  $\bar{W}$  of 3.19. This is 4.93 per cent higher than the value 3.04 of the optimal circular dimple.

For the geometries with asymmetric ‘V’, a possible mechanism of the lower leakage is that a part of the fluid tends to flow from the narrow edge to inner-driven by the high-pressure generated at the end of the narrow edge (Wang et al., 2018). The film pressure decreases from the end of the wide edge to the periphery, and it is further increased by the end of the narrow edge. In addition, fluid flows from the wide side to the narrow side of these two edges. The pressure is expected to be greatly increased at the edge ends according to the flow

Figure 1 Optimal shapes for the speed of 209 rad/s

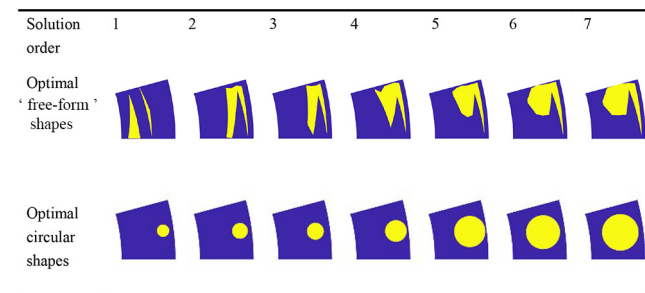
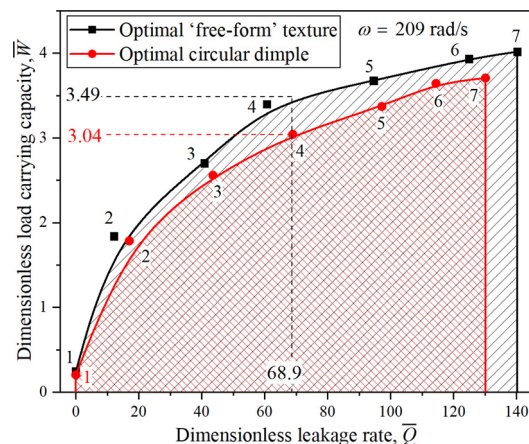


Figure 2 Multi-objective optimization solutions for the speed of 209 rad/s



continuity principle. This phenomenon is weaker for the circular dimple due to circle's smooth boundary. Thus, they have a higher load-carrying capacity.

### 2.3 Calculated coefficient of friction and leakage rate

The coefficient of friction (COF) and leakage rate are calculated for the optimal shapes for the following comparison with the experimental results. The opening force  $F_o$  (which is equivalent to the closing force  $F_c$ , i.e. the spring force  $F_s$  in experiments) is simplified by:

$$F_o = \int_0^{2\pi} \int_{r_1}^{r_2} p r dr d\theta \quad (2)$$

Note that the film thickness is given an initial value and then it changes to produce an opening force to balance the closing force. Once the film thickness is known, the leakage rate will be recalculated by equation (1), and the COF can be calculated by:

$$f = \frac{\int_0^{2\pi} \int_{r_1}^{r_2} \left( \frac{h}{2r} \frac{\partial p}{\partial \theta} + \frac{\mu \omega r}{h} \right) r dr d\theta}{F_c} \quad (3)$$

### 2.4 Experiment procedure

The stationary specimen is made of sintered graphite with I.D. = 36 mm and O.D. = 46.5 mm. Sintered graphite is a common mechanical seal material with a density of 1.82 g/cm<sup>3</sup>, the elasticity modulus of 28 GPa and the tensile strength of 55 MPa. The rotating specimen is made of 304 stainless steel with I.D.= 35.8 mm and O.D.= 46.8 mm. After the polishing processing, the roughnesses of a stationary specimen and rotating specimen are less than 0.02 and 0.04 μm, respectively. The flatness is not more than 0.3 μm to ensure the specimens fit well. Surface textures are fabricated on the sliding surface of the rotating specimen by lithography and electrochemical machining which can be seen in Zhang et al's (2013) research. The specimens are shown in Figure 3.

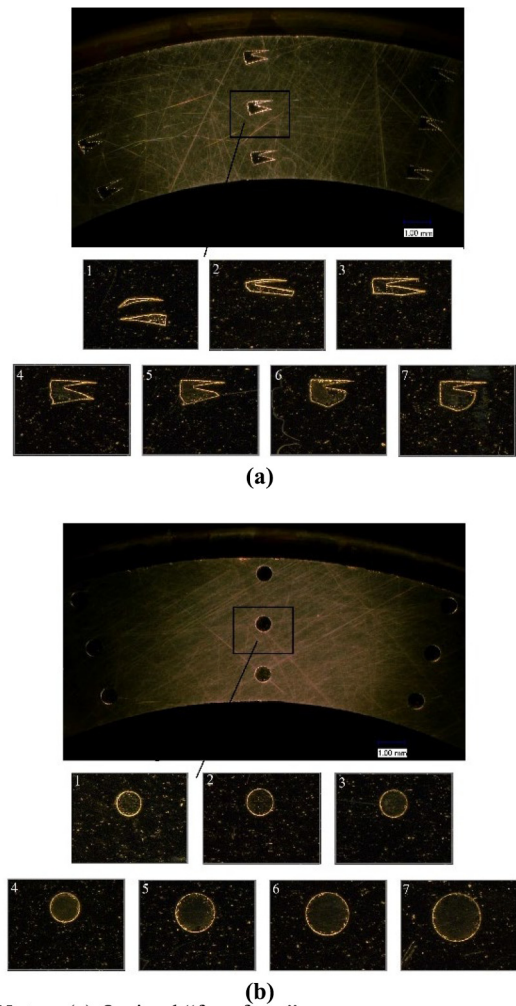
The experiments are conducted using a specialized test rig instrumented with sensors to measure load, leakage, friction torque, temperature and rotating speed. The schematic of the test rig is shown in Figure 4. The load is controlled by pressing a spring and is measured by a force sensor. The sealing medium is L-AN46, Newtonian fluid with dynamic viscosities of  $\mu = 40.25 \times 10^{-3}$  Pa·s at 40°C. It is connected with a tubule. The inner pressure is set to 0.12 MPa by controlling the liquid level in the tubule. Rubber rings and pads are added to ensure that leakage does not occur in addition to the interface of two specimens. The leakage rate is calculated by measuring the change in oil level. The friction torque was measured by a torque sensor attached on the stationary ring. Then, the friction coefficient  $f$  is calculated by the obtained friction torque. A 30-min running-in period is necessary to reach a steady state. Each experiment is repeated three times to ensure reliability.

## 3. Results and discussion

### 3.1 Comparison between calculated and experimental results

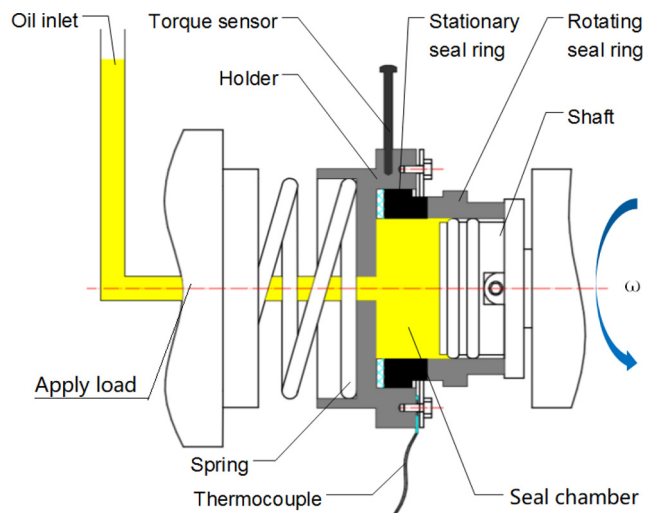
The results are presented in terms of a dimensionless parameter defined as  $\lambda = \frac{\mu \omega}{F_s / (\pi(r_2^2 - r_1^2))}$ . Taken the optimal "free-form" textures as an example, the calculated results and the

Figure 3 Images of textured specimens



Notes: (a) Optimal "free-form" textures; (b) optimal circular dimples

Figure 4 The schematic of the test rig



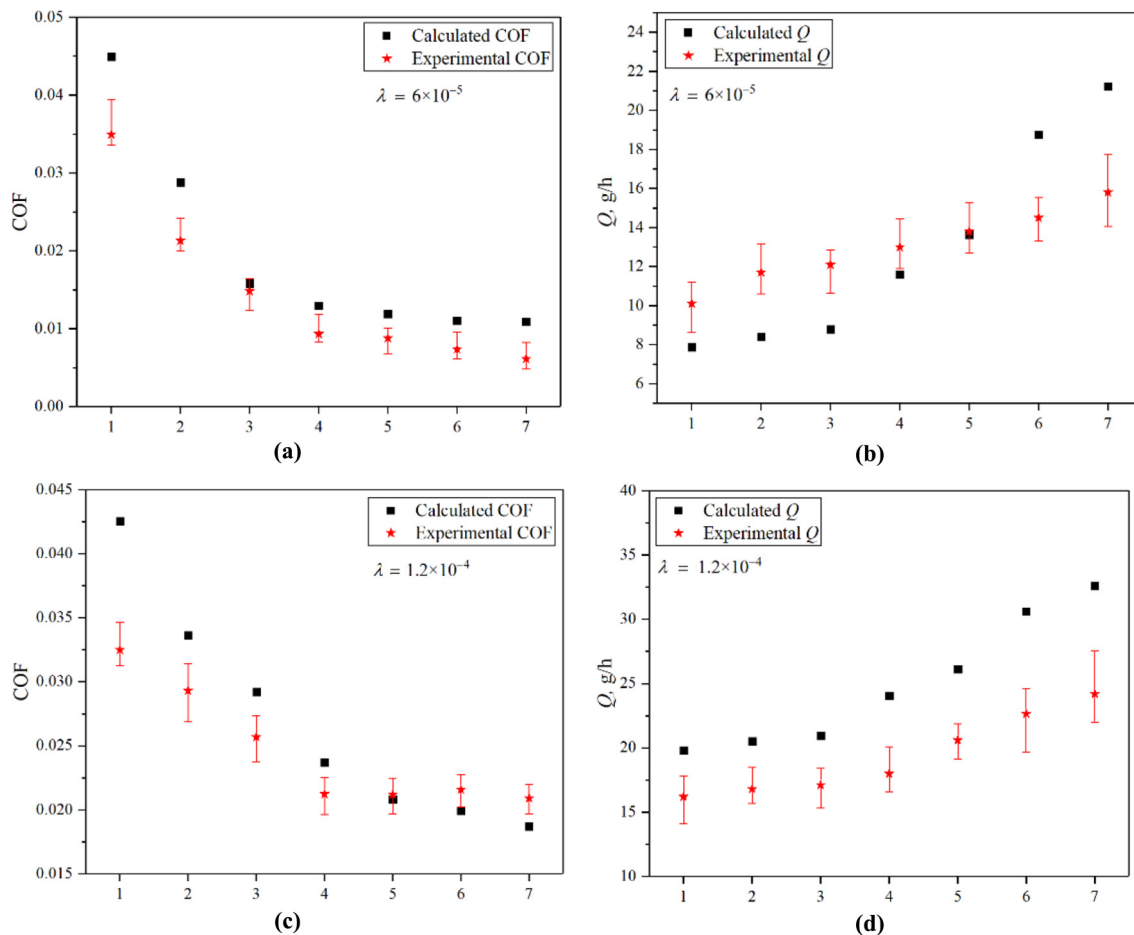
experimental results are compared for  $\lambda = 6 \times 10^{-5}$  and  $\lambda = 1.2 \times 10^{-4}$ .

Figure 5 shows the comparison between calculated results and experimental results. The point designation ★ refers to the average value of experiments and the upper limit and the lower limit of the error bar mean the maximum value and the minimum value in experiments, respectively. As shown in Figures 5(a) and (c), the COF decreases with the increasing solution order. The reason may be that: in the hydrodynamic lubrication regime, the friction comes from viscous shear force, according to the multi-objective optimization results, with the increasing solution order, the optimal shape can provide an increasing load-carrying capacity, then it will increase the film thickness and hence reduce the friction (Shen and Khonsari, 2016). In addition, the calculated COF is always larger than the experimental COF in most cases except for the Points 5, 6 and 7 in Figure 5(c). The possible reason is that: there exists a significant temperature rise (viscosity drop) especially for high speeds or heavy load. However, in the calculation, the viscosity is treated as a constant, which is larger than the actual value of the viscosity. This would result in a higher calculated COF according to equation (3). For the Points 5, 6 and 7, their experimental COFs are higher. This is likely due to the temperature rise is not obvious for large  $\lambda$  (high speed or light

load conditions). The simplifying assumption of no surface roughness causes the simulations to be in an ideal hydrodynamic lubrication state. However, the hydrodynamic lubrication state in experiments will turn into mixed lubrication due to the potential asperity contacts, which may lead to a higher experimental COF. The intersection of experimental COF and calculated COF in Figure 5(c) means the effects of multiply factors are not obvious or cancel each other out for this condition. Generally speaking, the calculated COF and experimental COF are in good agreement. Consideration of the surface roughness and thermal effect in further studies would improve the agreement.

As shown in Figures 5(b) and (d), the calculated and experimental leakage rate increase for the solution orders from one to seven. However, they differ greatly in value. For simulation, the simplifying assumptions of no surface roughness and no thermal effect will also lead to an error in calculated leakage. In experiments, there is always some oil that penetrates into the graphite ring, which makes the leakage rate higher than the actual value. Meanwhile, the leakage is increased greatly in occasionally unstable operation such as the vibration due to asperity contact in some cases, which makes the leakage rate larger than the actual value. The final deviation depends on the relationship of these factors. The intersection of

Figure 5 Calculated and experimental results



Notes: (a) COF for  $\lambda = 6 \times 10^{-5}$ ; (b) Q for  $\lambda = 6 \times 10^{-5}$ ; (c) COF for  $\lambda = 1.2 \times 10^{-4}$ ; (d) Q for  $\lambda = 1.2 \times 10^{-4}$

the experimental and calculated leakage means the deviation is small or the effects of multiply factors cancel each other out for this condition. In terms of their trends, the calculated and experimental leakages are considered to be consistent.

### 3.2 Comparison between optimal “free-form” texture and circular dimple

Figure 6 shows the calculated results and experimental results for different texture shapes. The number near the point is the solution order corresponding to Figure 1. As shown in Figure 6(a), the fitting curve of an optimal circular dimple is located above that of optimal “free-form” texture in most case. This implies that most of the optimal “free-form” textures show lower calculated COFs than the optimal circular dimple having a similar leakage rate. As shown in Figure 6(b), their experimental COFs are lower than those of optimal circular dimples with a similar leakage rate. The square black point means the experimental COF and leakage rate of a smooth specimen. It has the largest COF compared with the textured specimens, which is in accordance with the published paper (Marian et al, 2007). Although many textured specimens have a higher leakage rate than the smooth specimen, their COFs are reduced greatly. This is of great significance for working

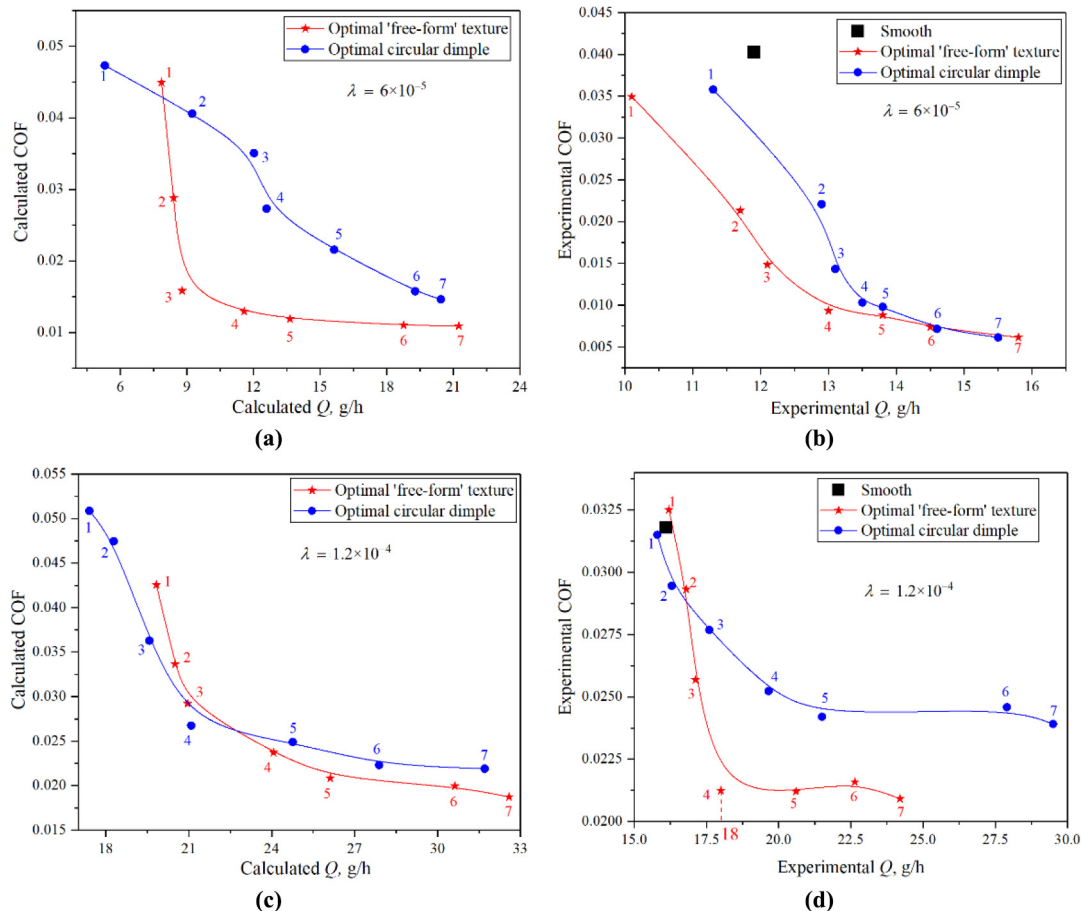
conditions where the leakage requirement is not critical. As can be seen in Figures 6(c) and (d), some optimal “free-form” textures show higher COFs for  $\lambda = 1.2 \times 10^{-4}$ . Not all optimal “free-form” textures perform a better combination performance than the optimal circular textures. The first and second optimal circular dimples could be applied for the working conditions with a critical leakage requirement. The fourth optimal “free-form” texture can be the best chosen when the leakage rate is allowed to exceed 18 g/h.

It should be noted that while the trends of calculated results and experimental results are similar, there is a large difference in values. This is because the error of leakage causes the curve to move in the horizontal direction and the error of COF causes the curve to move in the vertical direction. As a result, the combination of the two errors causes the experimental and calculated curves to appear to have a large discrepancy.

### 4. Conclusions

This study optimizes the shape of textures in mechanical seals using a multi-objective optimization approach. The obtained optimal “free-form” textures show a higher load-carrying capacity and a lower leakage rate than the optimal circular dimples in the simulation.

Figure 6 Comparison between optimal “free-form” textures and optimal circular dimples



Notes: (a) Calculated results for  $\lambda = 6 \times 10^{-5}$ ; (b) experimental results for  $\lambda = 6 \times 10^{-5}$ ; (c) calculated results for  $\lambda = 1.2 \times 10^{-4}$ ; (d) experimental results for  $\lambda = 1.2 \times 10^{-4}$

A series of experiments are conducted by constructing specimens made of the optimal textures. The experimental COF and leakage rate are in good agreement with the calculated results. Both the experiments and the calculations verified that the optimal “free-form” textures have a better combination performance in terms of a lower COF and a lower leakage than the optimal circular dimples in most cases.

## References

- Ahmed, A., Masjuki, H.H., Varman, M., Kalam, M.A., Habibullah, M. and Al Mahmud, K.A.H. (2016), “An overview of geometrical parameters of surface texturing for piston/cylinder assembly and mechanical seals”, *Meccanica*, Vol. 51 No. 1, pp. 9-23.
- Brunetière, N. and Tournerie, B. (2012), “Numerical analysis of a surface-textured mechanical seal operating in mixed lubrication regime”, *Tribology International*, Vol. 49 No. 11, pp. 80-89.
- Cem, S. (2009), “Investigation of load carriage capacity of journal bearings by surface texturing”, *Industrial Lubrication and Tribology*, Vol. 21 No. 5, pp. 261-270.
- Etsion, I. and Burstein, L. (1996), “A model for mechanical seals with regular microsurface structure”, *Tribology Transactions*, Vol. 39 No. 3, pp. 677-683.
- Gachot, C., Rosenkranz, A., Hsu, S.M. and Costa, H.L. (2017), “A critical assessment of surface texturing for friction and wear improvement”, *Wear*, Vols 372/373, pp. 21-41.
- Gachot, C., Rosenkranz, A., Reinert, L., Ramos-Moore, E., Souza, N., Müser, M.H. and Mücklich, F. (2013), “Dry friction between laser-patterned surfaces: role of alignment, structural wavelength and surface chemistry”, *Tribology Letters*, Vol. 49 No. 1, pp. 193-202.
- Galda, L., Pawlus, P. and Sep, J. (2009), “Dimples shape and distribution effect on characteristics of stribeck curve”, *Tribology International*, Vol. 42 No. 10, pp. 1505-1512.
- Gropper, D., Wang, L. and Harvey, T.J. (2016), “Hydrodynamic lubrication of textured surfaces: a review of modeling techniques and key findings”, *Tribology International*, Vol. 94, pp. 509-529.
- Ibatan, T., Uddin, M.S. and Chowdhury, M.A.K. (2015), “Recent development on surface texturing in enhancing tribological performance of bearing sliders”, *Surface and Coatings Technology*, Vol. 272, pp. 102-120.
- Kovalchenko, A., Ajayi, O., Erdemir, A., Fenske, G. and Etsion, I. (2005), “The effect of laser surface texturing on transitions in lubrication regimes during unidirectional sliding contact”, *Tribology International*, Vol. 38 No. 3, pp. 219-225.
- Marian, V.G., Kilian, M. and Scholz, W. (2007), “Theoretical and experimental analysis of a partially textured thrust bearing with square dimples”, *Proceedings of the Institution of Mechanical Engineers, Part J: Journal of Engineering Tribology*, Vol. 221, pp. 771-778.
- Qiu, Y. and Khonsari, M.M. (2011), “Experimental investigation of tribological performance of laser textured stainless steel rings”, *Tribology International*, Vol. 44 No. 5, pp. 635-644.
- Qiu, M., Minson, B.R. and Raeymaekers, B. (2013), “The effect of texture shape on the friction coefficient and stiffness of gas-lubricated parallel slider bearings”, *Tribology International*, Vol. 67 No. 4, pp. 278-288.
- Rahmani, R., Shirvani, A. and Shirvani, H. (2007), “Optimization of partially textured parallel thrust bearings with square-shaped micro-dimples”, *Tribology Transactions*, Vol. 50 No. 3, pp. 401-406.
- Shen, C. and Khonsari, M.M. (2016), “Texture shape optimization for seal-like parallel surfaces: theory and experiment”, *Tribology Transactions*, Vol. 59 No. 4, pp. 698-706.
- Shi, L., Wang, X., Su, X., Huang, W. and Wang, X. (2016), “Comparison of the load-carrying performance of mechanical gas seals textured with microgrooves and microdimples”, *Journal of Tribology*, Vol. 138, 021701-1-7.
- Siripuram, R.B. and Stephens, L.S. (2004), “Effect of deterministic asperity geometry on hydrodynamic lubrication”, *Journal of Tribology*, Vol. 126 No. 3, pp. 527-534.
- Tala-Ighil, N., Fillon, M. and Maspeyrot, P. (2011), “Effect of textured area on the performances of a hydrodynamic journal bearing”, *Tribology International*, Vol. 44 No. 3, pp. 211-219.
- Uddin, M.S., Ibatan, T. and Shankar, S. (2017), “Influence of surface texture shape, geometry and orientation on hydrodynamic lubrication performance of plane-to-plane slider surfaces”, *Lubrication Science*, Vol. 29 No. 3, pp. 153-181.
- Wan, Y. and Xiong, D. (2008), “The effect of laser surface texturing on frictional performance of face seal”, *Journal of Materials Processing Technology*, Vol. 197 Nos 1/3, pp. 96-100.
- Wang, T., Huang, W., Liu, X., Li, Y. and Wang, Y. (2014), “Experimental study of two-phase mechanical face seals with laser surface texturing”, *Tribology International*, Vol. 72, pp. 90-97.
- Wang, X., Shi, L., Dai, Q., Huang, W. and Wang, X. (2018), “Multi-objective optimization on dimple shapes for gas face seals”, *Tribology International*, Vol. 123, pp. 216-223.
- Yu, H., Wang, X. and Zhou, F. (2010), “Geometric shape effects of surface texture on the generation of hydrodynamic pressure between conformal contacting surfaces”, *Tribology Letters*, Vol. 37 No. 2, pp. 123-130.
- Zhang, H., Hua, M., Dong, G., Zhang, D. and Chen, W. (2017), “Optimization of texture shape based on genetic algorithm under unidirectional sliding”, *Tribology International*, Vol. 115, pp. 222-232.
- Zhang, B., Huang, W., Wang, J. and Wang, X. (2013), “Comparison of the effects of surface texture on the surfaces of steel and UHMWPE”, *Tribology International*, Vol. 65, pp. 138-145.

## Corresponding author

Xiaolei Wang can be contacted at: [xl\\_wang@nuaa.edu.cn](mailto:xl_wang@nuaa.edu.cn)

For instructions on how to order reprints of this article, please visit our website:

[www.emeraldgroupublishing.com/licensing/reprints.htm](http://www.emeraldgroupublishing.com/licensing/reprints.htm)

Or contact us for further details: [permissions@emeraldinsight.com](mailto:permissions@emeraldinsight.com)